REVIEW PAPER

Check for
updates

Uncertainty of volume fraction in bimrock using the scan-line method and its application in the estimation of deformability parameters

Yu-Chen Lu[1] · Yong-Ming Tien[1,2] · Charng Hsein Juang[1,2] · Jeen-Shang Lin[3]

Abstract

The volume fraction within a bimrock or bimsoil is an essential parameter that is useful for estimating the engineering properties of heterogeneous geomaterials. This paper presents analytical and numerical solutions to quantify the uncertainty of volume fraction measurements in bimrock/bimsoil using a scan-line method. The analytical solutions for the mean and variance of volume fraction estimates are based on a representative volume element model. The numerical solution is obtained through simulations of scan-line measurements. This work also employs physical tests using CT scan images from artificial bimrock/bimsoil to validate these solutions. The results demonstrate that the uncertainties of the volume fraction depend on the magnitude of the volume fraction of the blocks, the diameter of the blocks, and the length of the scan line. The proposed analytical and numerical solutions are compared with existing physical experimental tests and analytical solutions. An illustrative example to demonstrate the estimation of the uncertainty of volume fraction using the scan-line measurement is present. Finally, an example application of the volume fraction characterization in the geological engineering, in terms of Young's modulus estimation and characterization, is provided.

Keywords Bimrock · Bimsoil · Volume fraction · Scan-line method · Uncertainty · Representative volume element · Young's modulus

Introduction

The volume fraction (V_f) within a bimrock or bimsoil is an essential parameter that is useful for estimating the engineering characterization of heterogeneous geomaterials. The volume fraction plays an important role in the strength (Afifipour and Moarefvand 2014a; Barbero et al. 2008; Coli et al. 2011, 2012; Lindquist 1994; Lindquist and Goodman 1994; Medley 2001; Gokceoglu 2002; Kahraman and Alber 2006, 2008, 2009; Kalender et al. 2014; Sonmez et al. 2004, 2006a,

2016; Tien et al. 2015; Xia et al. 2017), deformability (Lindquist 1994; Lindquist and Goodman 1994; Kahraman and Alber 2006, 2009; Barbero et al. 2008; Afifipour and Moarefvand 2014a; Tien et al. 2015; Sonmez et al. 2004, 2006b, 2016; Xu et al. 2011; Tsesarsky et al. 2014), failure modes (Medley and Sanz Rehermann 2004; Afifipour and Moarefvand 2014b; Zhang et al. 2019), engineering properties (Medley and Sanz Rehermann 2004), or other physical properties (Kahraman et al. 2015) of geomaterials.

The V_f of interest could be the portion of discrete-phase inclusions (e.g., certain minerals, blocks, and particulates) or continuous-phase matrix in a composite material. In this study, the volume fraction of a block, V_b, is defined as the ratio of the block volume over the total volume, which is the same as the volumetric block proportion, VBP, established in some literature (Lindquist 1994; Lindquist and Goodman 1994; Kahraman and Alber 2006, 2008, 2009; Kahraman et al. 2015; Kalender et al. 2014; Medley 1994, 1997, 2001; Medley and Goodman 1994; Medley and Sanz Rehermann 2004; Sonmez et al. 2004, 2006a, b, 2016; Tsesarsky et al. 2014; Tien et al. 2010).

Measurements of V_f can be made through stereology and can be obtained via 0D, 1D, 2D, or 3D measurements

✉ Yong-Ming Tien
  ymtien@gmail.com

[1] Department of Civil Engineering, National Central University, No. 300, Zhongda Rd., Zhongli District, Taoyuan 32001, Taiwan

[2] Research Center for Hazard Mitigation and Prevention, National Central University, No. 300, Zhongda Rd., Zhongli District, Taoyuan, Taiwan

[3] Department of Civil and Environmental Engineering, University of Pittsburgh, 4200 Fifth Avenue, Pittsburgh, PA 15260, USA

depending on the dimension of the sampling windows used (Russ and Dehoff 1999). That is, 0D measurements are sampled by points, 1D by lines, 2D by areas, and 3D by volumes. Thus, "volume" is used in a generalized sense, with the resulting "volume" fraction being the ratio of the phase "volume" over the total volume sampled. That is, the volume fraction is defined as the point fraction, P_f, for 0D, the line fraction, L_f, for 1D, the area fraction, A_f, for 2D, and the volume fraction, V_f, for 3D. The Delesse principle (1847) shows that all these different dimensional measurements can lead to the same results, namely:

$$V_f = A_f = L_f = P_f. \tag{1}$$

It is difficult to determine the true volume fraction for bimrocks/bimsoils, especially for large scales. The common practice is to employ either 1D or 2D measurements, or both (Sonmez et al. 2004). Many investigators resolved to use aerial fractions of outcrops (2D surfaces), augmented with field and laboratory tests to obtain the geometric information of bimrock/bimsoil from outcrops (Medley 1994; Xu et al. 2008, 2011; Coli et al. 2012; Kahraman et al. 2015; Ymeti et al. 2017; Liu et al. 2018; Meng et al. 2018; Yang et al. 2019). However, it is not always possible to obtain areal fraction of blocks through image analysis if the blocks are dyed by matrix or the chromatism between blocks and matrix is small. As illustrated in Fig. 1, 1D measurement is perhaps the easiest and most efficient way to obtain an aerial fraction of block (A_b) in both laboratory and field scenarios. The 1D measurement has also been used for the estimation of area fraction A_f of a surface (i.e., a cross-section, an image), as in the estimation of lake area from remote sensing images (Stein and Yifru 2010) and air voids from concrete surface (ASTM 2012).

Further, according to the Delesse principle (1847), the expected value of A_b is equal to V_b if the sampling area is sufficiently large such that it can represent the geometry of true bimrocks/bimsoils. In this paper, we assume that scan-line measurements of the outcrops, images, or surfaces can reveal the 3D geometry of bimrocks/bimsoils. Accordingly, this paper uses V_b to express the areal fraction of block.

To avoid sampling bias, 1D lines sampling should be applied systematically. This is readily achieved using equally spaced, straight parallel lines (Fig. 1) that capture spatial variability within a given system. This systematic 1D line measurement is referred to herein as the scan-line method. To apply the scan-line method, the length of the sampling lines has to be selected, which may be estimated based on the confidence intervals. Quantification of the uncertainty in V_b is thus the first step to apply the scan-line method.

Various approaches have been proposed in the past to guide the selection of the required sampling length. For instance, some rules of thumb have been proposed. Holmes (1921) recommended that the total length of the lines be 100 times the average diameter of the grains being measured. Krumbein and Pettijohn (1938) considered that a total traverse length equal to 1000 times the largest particle would give a fair degree of accuracy. ASTM C457-11 (2012) requires the line length to be 1000 to 3000 times the maximum diameter of the void. Analytical solutions provide improved recommendations, but so far are limited to the cases where V_f is small. Hilliard and Cahn (1961) presented an analytical solution, which is only valid when the V_f of a void is less than 5%, as follows:

$$CV(V_f) = CV(L_c) \sqrt{\frac{L}{E(L_c)\left[CV(L_c)^2 + 1\right]}} = \sqrt{\frac{1}{E(L_c)}} \tag{2}$$

where $E(\cdot)$ represents the expected value, $CV(\cdot)$ represents the coefficient of variance, L indicates the total length of the scan line, and L_c is the length of the interception when the scan line passes through a void. If the particle shape is circular, Eq. (2) can be simplified as follows:
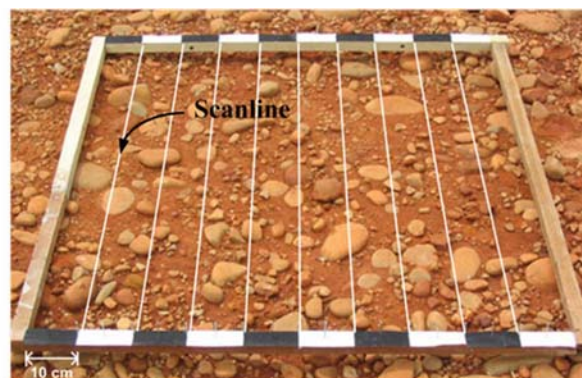
Fig. 1 Scan line(s) measured on an outcrop. **a** Graphic model of mélange (Medley 1994). **b** Lateritic gravel formation, Taoyuan, Taiwan (Kuo 2005)

$$CV(V_{\mathrm{f}}) = CV(V_{\mathrm{f}})\sqrt{\frac{L}{D_{\mathrm{e}}}} = \sqrt{\frac{8}{3\pi E(V_{\mathrm{f}})}} \qquad (3)$$

Medley and Goodman (1994) developed empirical solutions. They applied hand-tracing on a photograph of mélange cores to evaluate the convergence of V_{b} with respect to the scan-line sampling lengths. Medley (1994) further prepared a series of bimrock samples when investigating the uncertainty associated with volume fraction estimation, with the known V_{b} varying within the range of 13 to 55%. Medley further developed a chart to determine the uncertainty factor for various scan-line lengths and V_{b} (Medley 1997, 2001).

In the following, the concept of "represented volume element," or RVE, is introduced first. A new analytical solution on V_{b} measurement uncertainty that is based on RVE is then presented. This is followed a detailed description of the verification efforts. The verification is carried out first by numerical simulation and further by applying to controlled physical tests. A new empirical equation is derived from the numerical simulation results. Finally, an example is presented for estimation of the uncertainty of volume fraction; the results are further used to estimate the deformability parameters, including the shear modulus and Young's modulus.

Methodology: analytical solution and numerical simulation

Representative volume element

The measurement of the volume fraction of inclusions within a rock matrix is used as an example for introducing the RVE concept. Consider the case that circular inclusions of the same size are randomly and uniformly distributed within a 2D matrix, RVE can be thought of a square element with a circular inclusion that has a volume fraction within the element the same as V_{b} to be measured. A randomly drawn scan line, as shown in Fig. 2, would repeatedly hit and miss the inclusions. If the RVE is superimposed and aligned with the nearby circular inclusion that intersects with the scan line, as depicted in Fig. 2, it becomes clear that estimates of V_{b} using scan lines can conceptually be obtained by simply studying a single RVE. When the blocks are uniformly and randomly distributed within a matrix, a straight line of length L becomes N line segments randomly drawn inside the RVE, where NL_{s} equals L and L_{s} is the width of the RVE. From this, a theoretical derivation makes it possible to estimate V_{b} using random variables.

It is important to note that RVE, the natural of the phase, inclusion determines how high V_{b} can go. For instance, in a 2D setting with uniform circular inclusions

the maximum V_{b} that can be attained is 78.5% (= $\pi r^2/(2R)^2$) when the circular inclusions circumscribe the boundary of RVE. While in a 3D setting, since a sphere circumscribes to the boundary of a cube RVE can work with V_{b} only up 52.4% (= $4/3\pi r^3/(2R)^3$). But in reality, these limits can be broken when the inclusions have different sizes. To model that, the inclusions should be composed of polydisperse circle or spheres within an RVE. Such formulations are presented also.

Mathematical derivation

The analytical solution is first derived with the following considerations (assumptions): (i) The inclusions are circular; (ii) the scan lines are assumed to be vertical within a RVE; (iii) the inclusions distribution within the matrix follows isotropic, uniform, and random (called IUR) conditions; (iv) the RVE is square with a width L_{s}, contains a circular inclusion of diameter D; (v) the value of V_{b} is in the range of 0 to $\pi/4$." It thus gives the expected V_{b}

$$E_{RVE}(V_{\mathrm{b}}) = \frac{\pi D^2}{4L_{\mathrm{s}}^2}, \text{where } 0 \leq E_{REV}(V_{\mathrm{b}}) \leq \pi/4. \qquad (4)$$

From the RVE model (Fig. 3), a scan line passing through x would intercept the inclusion with an intercept length, L_{c}, as follows,

$$\begin{cases} L_{\mathrm{c}} = 2\sqrt{\frac{D^2}{4} - x^2}, & -\frac{D}{2} \leq x \leq \frac{D}{2} \\ L_{\mathrm{c}} = 0, & \text{otherwise} \end{cases}. \qquad (5)$$

The relationship of L_{c} with V_{b} is simply

$$V_{\mathrm{b}} = E_{RVE}(L_{\mathrm{b}}) = \frac{E_{RVE}(L_{\mathrm{c}})}{L_{\mathrm{s}}}, \text{where } 0 \leq V_{\mathrm{b}} \leq \pi/4, \qquad (6)$$

which further gives

$$E_{RVE}(L_{\mathrm{c}}) = \frac{\pi D^2}{4L_{\mathrm{s}}}. \qquad (7)$$

The variance of linear fraction of block (L_{b}) in an RVE, $V_{REV}(L_{\mathrm{b}})$ can be expressed by

$$V_{RVE}(L_{\mathrm{b}}) = E_{RVE}(L_{\mathrm{b}}^2) - E_{RVE}(L_{\mathrm{b}})^2, \text{where } 0 \leq E_{REV}(L_{\mathrm{b}}) \leq \pi/4. \qquad (8)$$

And Eq. (8) can also be expressed by L_{c} and L_{s} as shown as follows:

$$V_{RVE}(L_{\mathrm{b}}) = \frac{\int_0^{L_{\mathrm{s}}} \left(\frac{L_{\mathrm{c}}}{L_{\mathrm{s}}}\right)^2 dx}{\int_0^{L_{\mathrm{s}}} dx} - \left[\frac{\int_0^{L_{\mathrm{s}}} \left(\frac{L_{\mathrm{c}}}{L_{\mathrm{s}}}\right) dx}{\int_0^{L_{\mathrm{s}}} dx}\right]^2. \qquad (9)$$

Fig. 2 Conceptual diagram of an RVE model
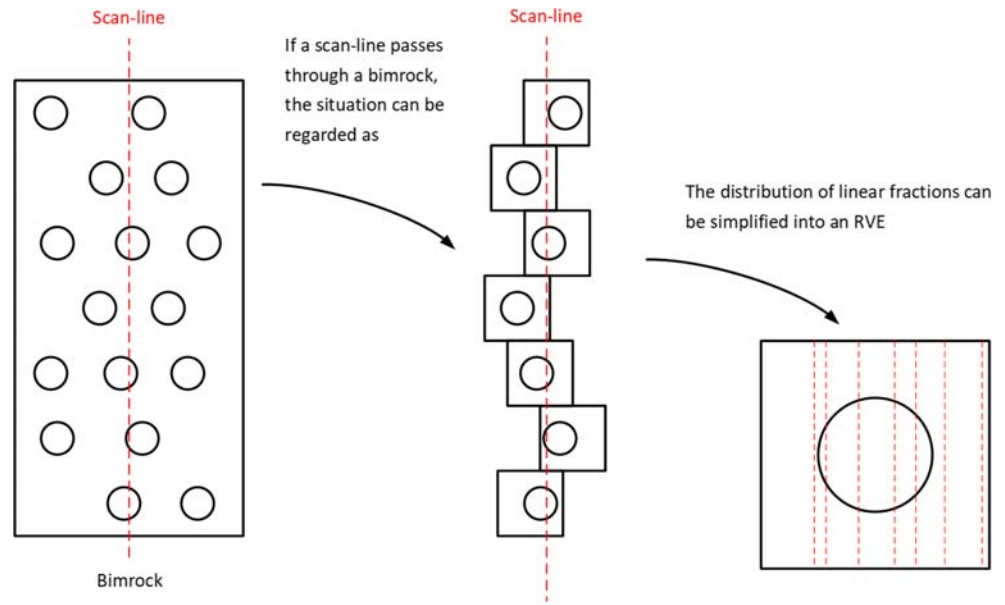
And Eq. (9) can be rewritten as

$$V_{RVE}(L_f) = \frac{D}{L_s^3}\left[E_{RVE}\left(L_c^2\right) - \frac{D}{L_s}E_{RVE}(L_c)^2\right]. \tag{10}$$

Substituting Eq. (7) into Eq. (10), Eq. (10) can be represented using L_c and L_b, as follows:

$$V_{RVE}(L_b) = \frac{\sqrt{\pi}}{2}\frac{E_{RVE}\left(L_c^2\right)}{E_{RVE}(L_c)^2}E_{RVE}(L_b)^{\frac{3}{2}} - E_{RVE}(L_b)^2, \tag{11}$$

$$\text{where } 0 \leq E_{REV}(L_b) \leq \pi/4.$$

Fig. 3 Mathematical model of an RVE

As shown in Fig. 2, each scan line can be viewed as a summation process. Thus, the statistics of its L_b will converge to a Gaussian distribution, which can be explained through the central limit theorem (CLT) (Wackerly et al. 2008). The mean value and uncertainty of L_b estimation at various sampling sizes ($N = L/L_s$) can be determined as follows:

$$E(L_b) = E_{RVE}(L_b)$$
$$V(L_b) = \frac{1}{N}V_{RVE}(L_b), \text{ where } 0 \leq E(L_b) \leq \pi/4, \tag{12}$$

where $V(\cdot)$ represents variance.

By substituting Eq. (6) and Eq. (11) into Eq. (12), the following is obtained:

$$V(L_b) = \frac{1}{L}\left\{\left[\frac{E\left(L_c^2\right)}{E(L_c)}\right]E(L_b) - \frac{2E(L_b)^{\frac{3}{2}}E(L_c)}{\sqrt{\pi}}\right\}, \text{ where } 0 \leq E(L_b) \leq \pi/4. \tag{13}$$

Equation (13) can determine the uncertainty of the linear fraction of a block by accessing the length of the scan line, the intercept lengths, and the expected linear fraction of the block, which can be obtained from a scan-line measurement.

Although a block diameter cannot be measured directly using the scan-line method, D can be calculated using Eq. (7). Hence, Eq. (13) can be rewritten as

$$V(L_b) \times \frac{L}{D} = \frac{8}{3\pi}E(L_b) - \frac{\sqrt{\pi E(L_b)^3}}{2}, \text{ where } 0 \leq E(L_b) \leq \pi/4. \tag{14}$$

Equation (14) is the same as the analytical solution proposed by Tien et al. (2010), which can estimate the uncertainty of a scan-line measurement under monodisperse block inclusion.
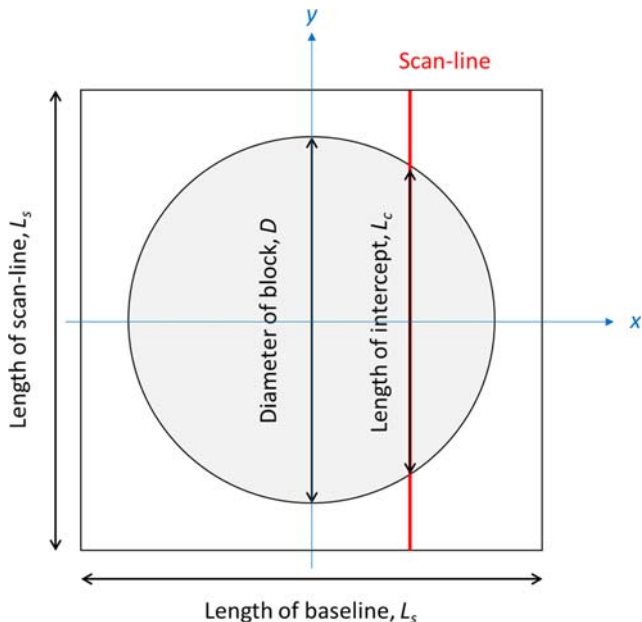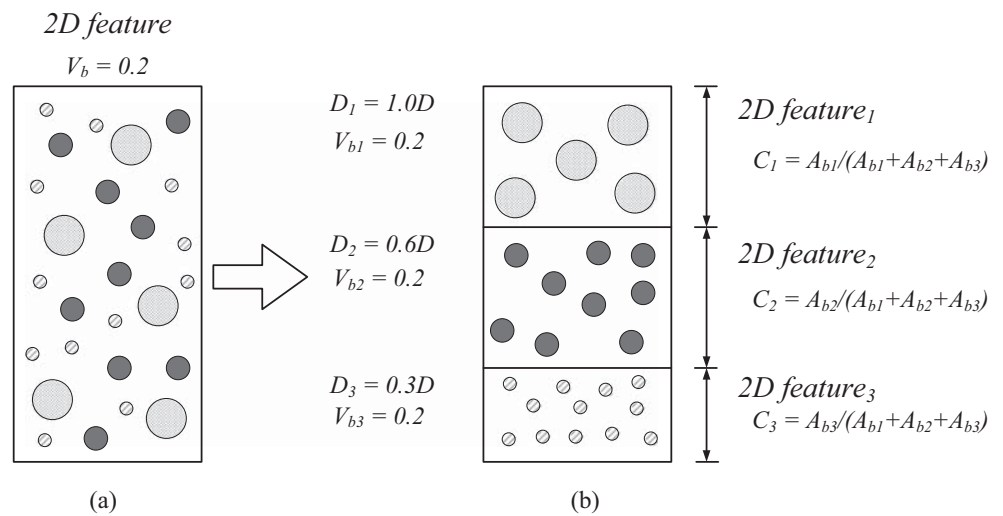
Fig. 4 Conceptual diagram of tackling polydisperse inclusions

(a)

(b)

Most block dispersions are polydisperse. Clearly, Eq. (13) or Eq. (14) cannot be used under this condition. To tackle this issue, this study employs the concept of the "total sum of squares" (*TSS*) (Wackerly et al. 2008), which includes the "sum of squares for treatment" (*SST*, the first term of Eq. (15)), and the "sum of squares for error" (*SSE*, the second term of Eq. (15)), where SST can be viewed as the measurement uncertainty from the block size variability and *SSE* can be viewed as the measurement uncertainties from the spatial probability of each block size:

$$TSS = n \sum_{i=1}^{k} \left(\overline{Y}_i - \overline{Y} \right)^2 + \sum_{i=1}^{k} \sum_{j=1}^{n} \left(Y_{ij} - \overline{Y} \right)^2. \tag{15}$$

A polydisperse inclusion (Fig. 4a) can be reassembled as shown in Fig. 4b, with each block size having the same A_f, indicating there are no A_f variations between each block size. Thus, the *SST* is equal to zero, and the *TSS* is equal to the *SSE*. Hence, Eq. (15) can be rewritten as:

$$TSS = \sum_{i=1}^{k} \sum_{j=1}^{n_i} [L_{b\,ij} - E(L_b)]^2 = \sum_{i=1}^{k} n_i V(L_b). \tag{16}$$

Then, the total number of measurements in Eq. (16) is divided, which can be rewritten as follows:

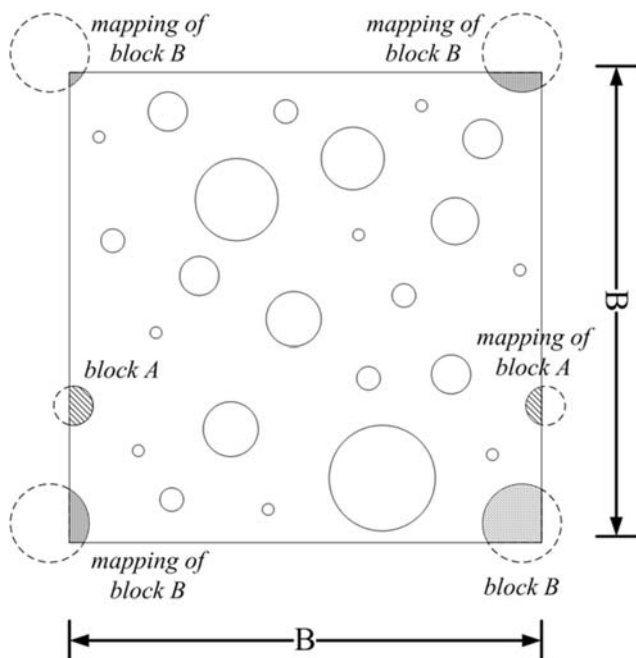$$V_{\mathrm{TSS}}(L_b) = \int V(L_b) f(\mathrm{d}) \mathrm{d}\mathrm{d} \tag{17}$$

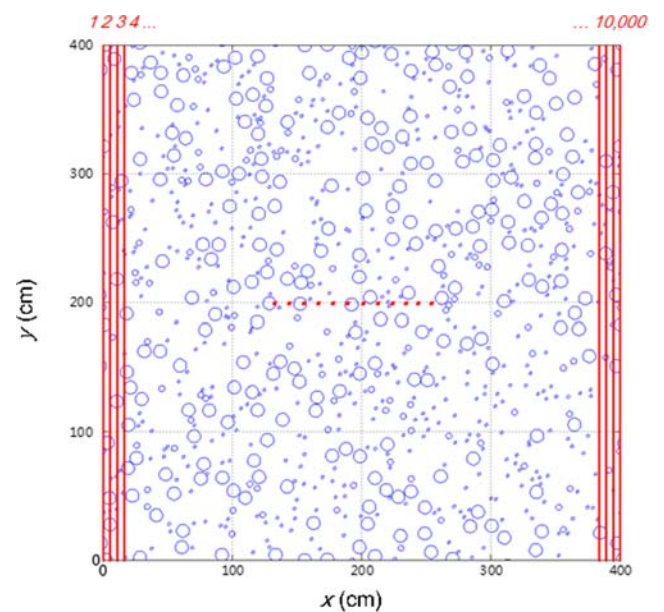Fig. 5 Conceptual diagram of the periodic boundary

Fig. 6 Scan lines for determining the uncertainty of V_b estimation through a statistical approach

Table 1 Parametric studies for numerical simulations

Volume fraction of block, V_b (%)	Length of scan line, L/D_e	Block proportion[a], $C_1:C_2:C_3$	Block size, D
3.14, 6.28, 12.6, 25.1, 37.7, 50.3	30, 60, 120, 240	0:1:0	5 cm
4.71, 9.43, 18.9, 28.3, 37.8, 47.1, 56.5	30, 60, 120, 240	10:1:1, 3:2:1, 1:1:1, 1:1:10	10 cm, 5 cm, 2.5 cm

[a] Block proportion $C_1:C_2:C_3$ of block diameters equal to 10 cm, 5 cm, and 2.5 cm, respectively.

where $f(d)$ represents the possibility density function of intercepts from the ith block size, which can also be represented as the block proportion, $Ci = i$th block area / total block area.

Substituting Eq. (14) into Eq. (17), and allowing the *TSS* to have an equivalent diameter, D_e, the following is obtained:

$$D_e = \int D f(d) dd. \tag{18}$$

Equation (18) can also be expressed in series as follows:

$$D_e = \sum_{i=1}^{n} C_i D_i. \tag{19}$$

Substituting Eq. (7) into Eq. (18), the resulting equation can be rewritten as:

$$D_e = \frac{4}{\pi} \int E(L_c) f(d) dd. \tag{20}$$

Assuming that for each block $E(L_c) = a_i E(L_c)_{eq}$, where a_i is a multiple factor based on the equivalent block size and $E(L_c)_{eq}$ is an equivalent intercept mean, Eq. (15) can then be rewritten as

$$D_e = \frac{4}{\pi} \frac{\int \left[a E(L_c)_{eq} \right] a da}{\int a^2 da} = \frac{4}{\pi} E(L_c)_{eq}. \tag{21}$$

The results of Eq. (21) are the same as those of Eq. (7), which means Eq. (13) can be used to determine the uncertainty of L_b in polydisperse inclusions. In addition, Eq. (14) should be rewritten as follows:

$$V(L_b) \times \frac{L}{D_e}$$
$$= \frac{8}{3\pi} E(L_b) - \frac{\sqrt{\pi E(L_b)^3}}{2}, \text{ where } 0 \leq E(L_b) \leq \pi/4. \tag{22}$$

For a reliability design or other in situ investigations, most engineers apply $CV = \sqrt{V(.)}/E(\cdot)$ to determine the uncertainty of the measurement. Equations (13) and (22) can therefore also be presented as a *CV*, which are expressed as

$$CV(L_b) = \sqrt{\frac{1}{L} \left\{ \left[\frac{E(L_c^2)}{E(L_c)} \right] \frac{1}{E(L_b)} - \frac{2E(L_c)}{\sqrt{\pi E(L_b)}} \right\}}, \tag{23}$$

$$CV(L_b) \sqrt{\frac{L}{D_e}} = \sqrt{\frac{8}{3\pi E(L_b)} - \sqrt{\frac{\pi}{4E(L_b)}}}, \tag{24}$$

where $0 \leq E(L_b) \leq \pi/4$, $D_e = \sum_{i=1}^{n} C_i D_i$, or $D_e = \frac{4}{\pi} E(L_c)$.

Equations (23) and (24) present an analytical solution for the uncertainty of the volume fraction measurements using scan-line method. This analytical solution is applicable when $E(L_b)$ is in the range of $0 \leq E(L_b) \leq \pi/4$.

Numerical simulations

This paper presents a MATLAB code that can address a volume fraction measurement in a bimrock/bimsoil using a scan line. A 2D domain with uniform and random circular block dispersions in a square domain was generated. A series of scan lines were placed on the feature. A series of L_b were obtained. The mean and standard deviation of L_b were calculated.

Periodic boundary

While generating the 2D domain, it is impossible to avoid wall (or edge) effects (Bentz and Garboczi 1999), which result in non-uniform dispersion near the edges. To reduce the effect of the edge, four strips (2D in width) were trimmed from the four edges of an extended square (the generated domain) (Tien et al. 2010). However, this approach may result in V_b scatter. To tackle this issue, a periodic boundary is applied in this study. If a block intersects one edge of the boundaries, the outside part of the block will be mapped onto its opposite side, as shown in Fig. 5. The advantages of the periodic boundary method are to eliminate the wall effect and to generate features with the precisely desired volume fraction.

Fig. 7 Histograms of linear fractions of blocks measured by various scan-line lengths (L/D_e = 30, 60, 120, 240) for **a–d** V_b = 0.05 and **e–h** V_b = 0.5
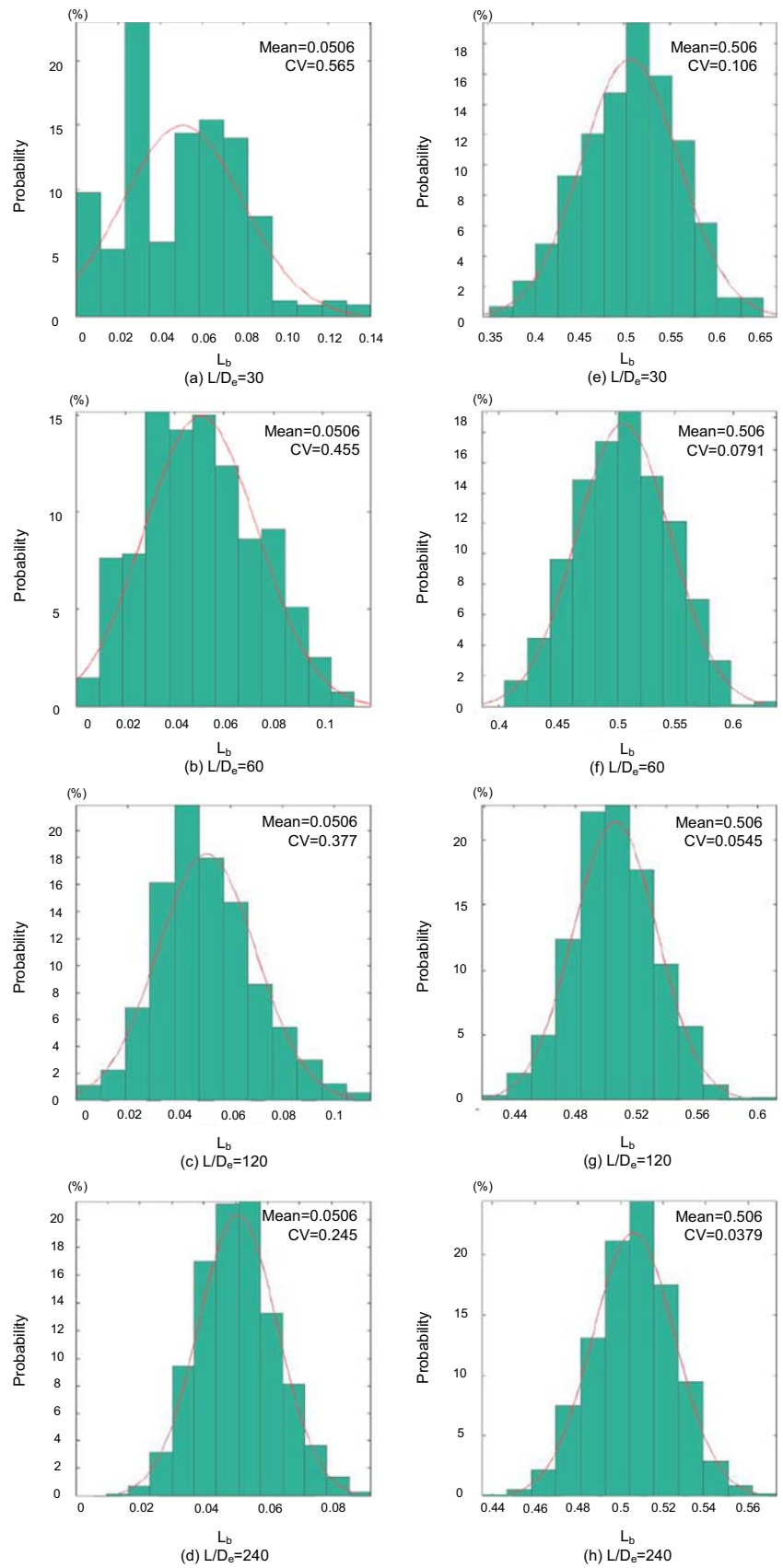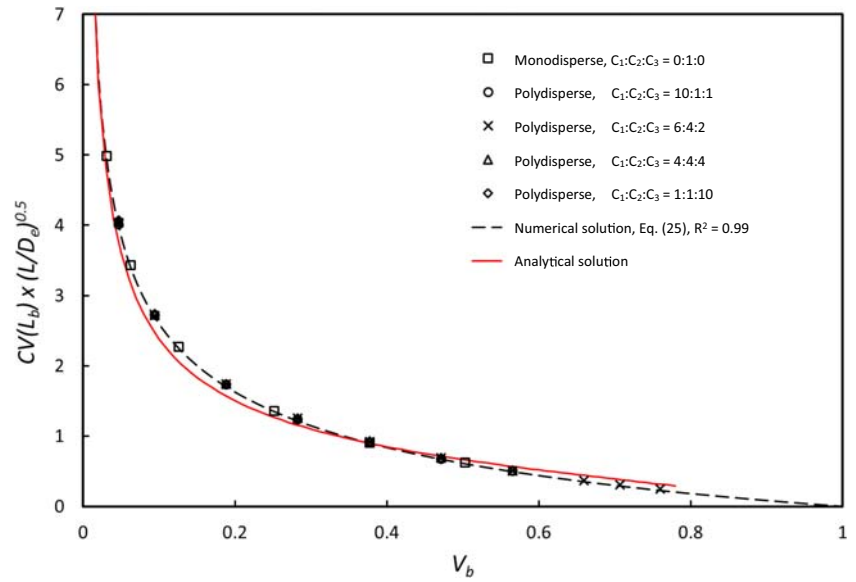

(a) L/D$_e$=30

(b) L/D$_e$=60

(c) L/D$_e$=120

(d) L/D$_e$=240

(e) L/D$_e$=30

(f) L/D$_e$=60

(g) L/D$_e$=120

(h) L/D$_e$=240

Fig. 8 Normalized coefficients of
variance $(CV(L_b)(L/D_e)^{0.5})$ vs
volumetric fraction (V_b)

Sizes of domain and block

The size of the domain should be sufficiently large to
accommodate a large number of blocks embedded into
the matrix to meet the conditions of being statistically
isotropic and homogeneous. In this study, the size of the
domain is 400 cm × 400 cm. The diameters of the blocks
are 2.5 cm, 5 cm, and 10 cm.

Simulation procedures

The numerical simulation procedures are as follows:

I.   Define a square domain of size B × B
II. Determine V_b within this domain

III. Place circular blocks randomly, and do not allow any
     overlap between blocks
IV. Generate a large number of scan lines (say 10,000) in
     Fig. 6. Then, calculate linear fractions of blocks, L_b, for
     each line

Repeat steps (1) through (4) 100 times for each V_b; thus, this
work regenerates a heterogeneous rock mass 100 times for each
V_b and calculates the total mean L_b (100 × 10,000) and CV.

Parametric studies

Parametric studies were performed to evaluate the effects on
the uncertainty of volume fraction estimation. Several

Fig. 9 Block size distribution of
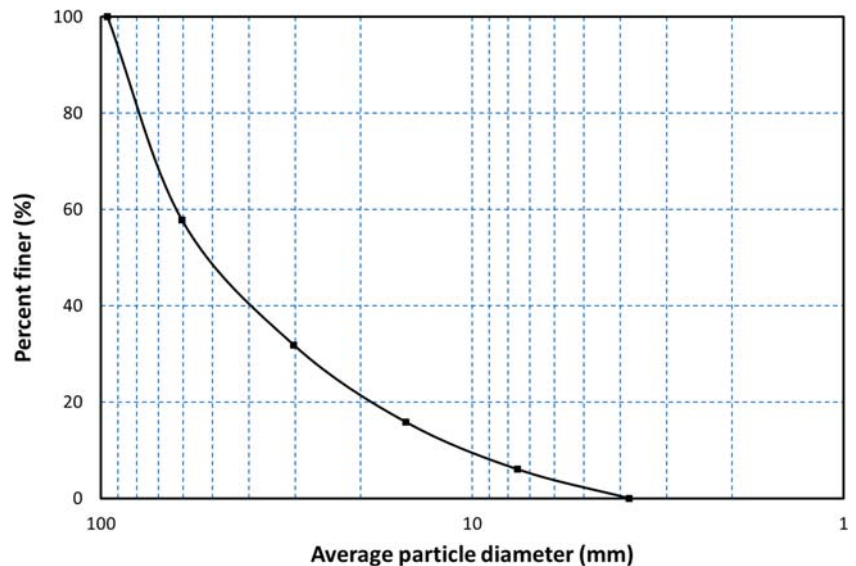Medley's (1997) physical model
tests

Table 2 Block size distribution of Medley's (1997) physical model

Elliptical block size (a:b:c)	Average diameter[a] (D_{3D})	Percentage of block number	Block proportion (C_i)
6:3:3 mm	3.78 mm	79.7%	6.04%
12:6:6 mm	7.56 mm	16.2%	9.83%
24:12:12 mm	15.1 mm	3.29%	16.0%
48:24:24 mm	30.2 mm	0.668%	25.9%
96:48:48 mm	60.5 mm	0.136%	42.2%

[a] $D_{3D} = \sqrt[3]{abc}$

[b] $D_e = \frac{9\pi}{32} \sum\limits_{i=1}^{5} C_i D_{3D_i} = \frac{9\pi}{32}(3.78 \times 0.0604 + 7.56 \times 0.0983 + 15.1 \times 0.16 + 30.2 \times 0.259 + 60.5 \times 0.422) = 32.5$ mm

parameters, block sizes, relative lengths of scan lines, L/D_e, and volume fractions of blocks, V_b, were selected. Three block sizes were used: $D_1 = 10$ cm, $D_2 = 5$ cm, and $D_3 = 2.5$ cm, including monodisperse and polydisperse types. Four different relative lengths of scan lines (L/D_e) were studied, including $L/D_e = 30$, $L/D_e = 60$, $L/D_e = 120$, and $L/D_e = 240$. The range of V_b is from 3.14 to 70.1%. The parameters for the simulated bimrock/bimsoil are as shown in Table 1.

Simulation results

Parametric study for the relative length of a scan line The simulation results are shown in Fig. 7. Cases of lower and higher V_b are given as examples. It can be clearly seen that V_b affects the uncertainty and distribution of L_b even under the same dimensionless length of a scan line (or sampling size). For lower V_b (= 0.0506) (shown in Fig. 7a as a lower dimensionless length of a scan line, $L/D_e = 30$), the distribution of L_b shows a non-normal or a non-log-normal distribution. As L/D_e increases, the distribution becomes more similar to a normal distribution, as

shown in Fig. 7a–d. For higher V_b (= 0.506) for $L/D_e = 30$ (shown in Fig. 7a), the distribution of L_b has an approximately normal distribution. The CV of L_b is inversely proportional to the square root of L/D_e, which can be predicted by the analytical solution (Eq. (19)) and explained based on the CLT.

Equivalent diameter of the blocks For polydisperse cases, the equivalent diameter of the blocks can be calculated using Eq. (19). For example, the diameters of blocks D_1, D_2, and D_3 are 10 cm, 5 cm, and 2.5 cm, respectively, and the ratio of block proportions is $C_1:C_2:C_3 = 6:4:2$. The equivalent diameter of the block is

$$D_e = 10 \times 6/12 + 5 \times 4/12 + 2.5 \times 2/12 = 7.08\,\text{m}.$$

There is a correlation between the measurement uncertainty and block sizes, as shown in Eq. (19). From previous parametric studies, the uncertainty is proportional to the square root of the sampling size. Therefore, $CV(L_b)$ multiplied by (L/D_e) could be a constant at a particular V_b. Other similar

Fig. 10 CVs of the volume fraction measured from Medley's (1997) model and the present study
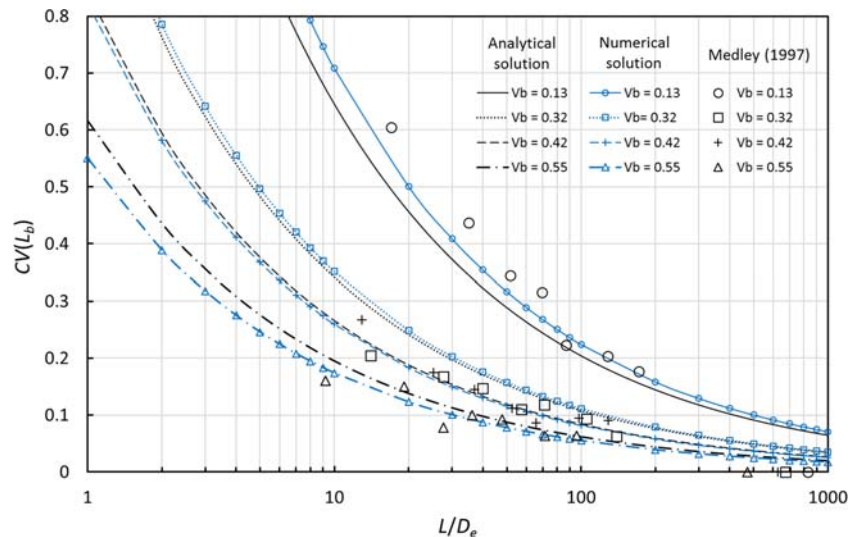
Table 3 *CVs* of block volume fractions: experimental data, analytical solutions, and numerical solution

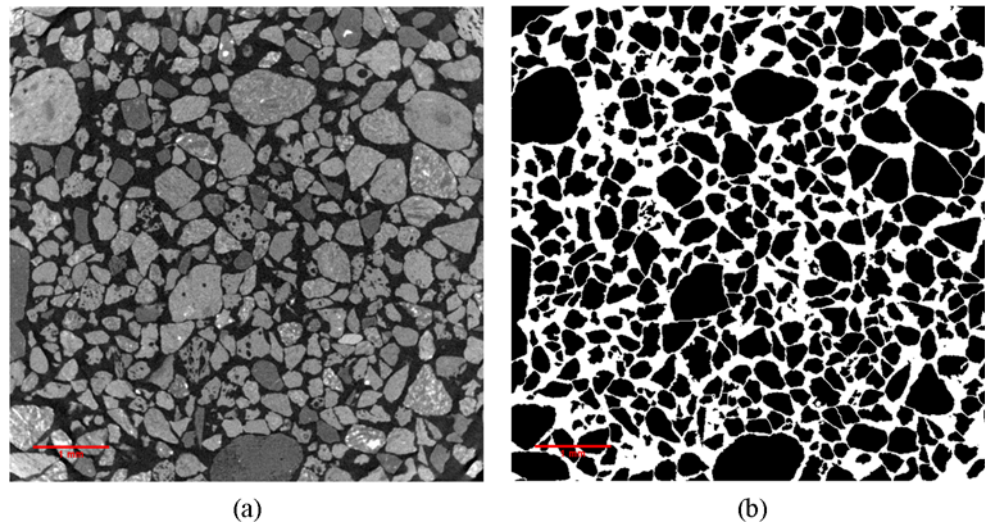| | Volume fraction of blocks, V_b | Equivalent diameter, D_e (cm) | Length of scan line, L/D_e | $CV(L_b)(L/D_e)^{0.5}$ | | This study | |
				Experimental data	Hilliard and Cahn (1961)	Analytical solution	Numerical solution
Medley's (1997) physical model	0.13	3.25	17–830	2.11	2.55	2.01	2.24
	0.32	3.25	14–672	0.762	1.63	1.04	1.10
	0.42	3.25	13–627	0.773	1.42	0.883	0.807
	0.55	3.25	9–472	0.495	1.24	0.590	0.536
Case I	0.554	0.366	16.9	0.582	1.24	0.585	0.530
Case II	0.505	0.0698	27.9	0.617	1.30	0.659	0.620
Case III	0.417	0.0707	27.5	0.770	1.43	0.814	0.814
Case IV	0.300	0.0700	27.9	1.23	1.68	1.10	1.17
Case V	0.179	0.0637	30.6	1.64	2.18	1.80	1.79
Case VI	0.103	0.0698	27.9	2.43	2.87	2.34	2.59
Case VII	0.0452	0.0704	27.7	4.05	4.33	3.82	4.12

studies (Tien et al. 2010, 2011, 2012, 2015) also concluded this phenomenon.

A parametric study of block sizes is shown in Fig. 8. All the uncertainties of V_b estimations for the various block sizes are located on a curved line. This means the numerical simulations for various block sizes followed Eq. (19).

Regression curve for numerical solutions Based on the results of the numerical simulations, a relationship between CV, V_b, and L/D_e was obtained via a regression procedure ($R^2 = 0.99$):

$$CV\sqrt{L/D_e} = 0.259(\log V_b)^4 + 0.242(\log V_b)^3 - 0.734(\log V_b)^2 - 1.88(\log V_b) \tag{25}$$

A comparison of the analytical and numerical solutions is shown in Fig. 8.

Validation: physical model test and CT scan images

The results of the physical model developed by Medley (1997) and the CT scan images are adapted to validate the analytical and numerical solutions.

Physical model

The physical bimrock models were composed of plaster of Paris matrices in which were embedded ellipsoidal blocks to

Fig. 11 Cross-sectional images of the Iceland sand sample. **a** Original CT scan image. **b** Binary image (case I)

(a)   (b)

Fig. 12 CT scan images of crushed rock. **a** V_b = 50.5%. **b** V_b = 41.7%. **c** V_b = 30.0%. **d** V_b = 17.3%. **e** V_b = 10.3%. **f** V_b = 4.51%


(a)

(b)

(c)

(d)

(e)

(f)
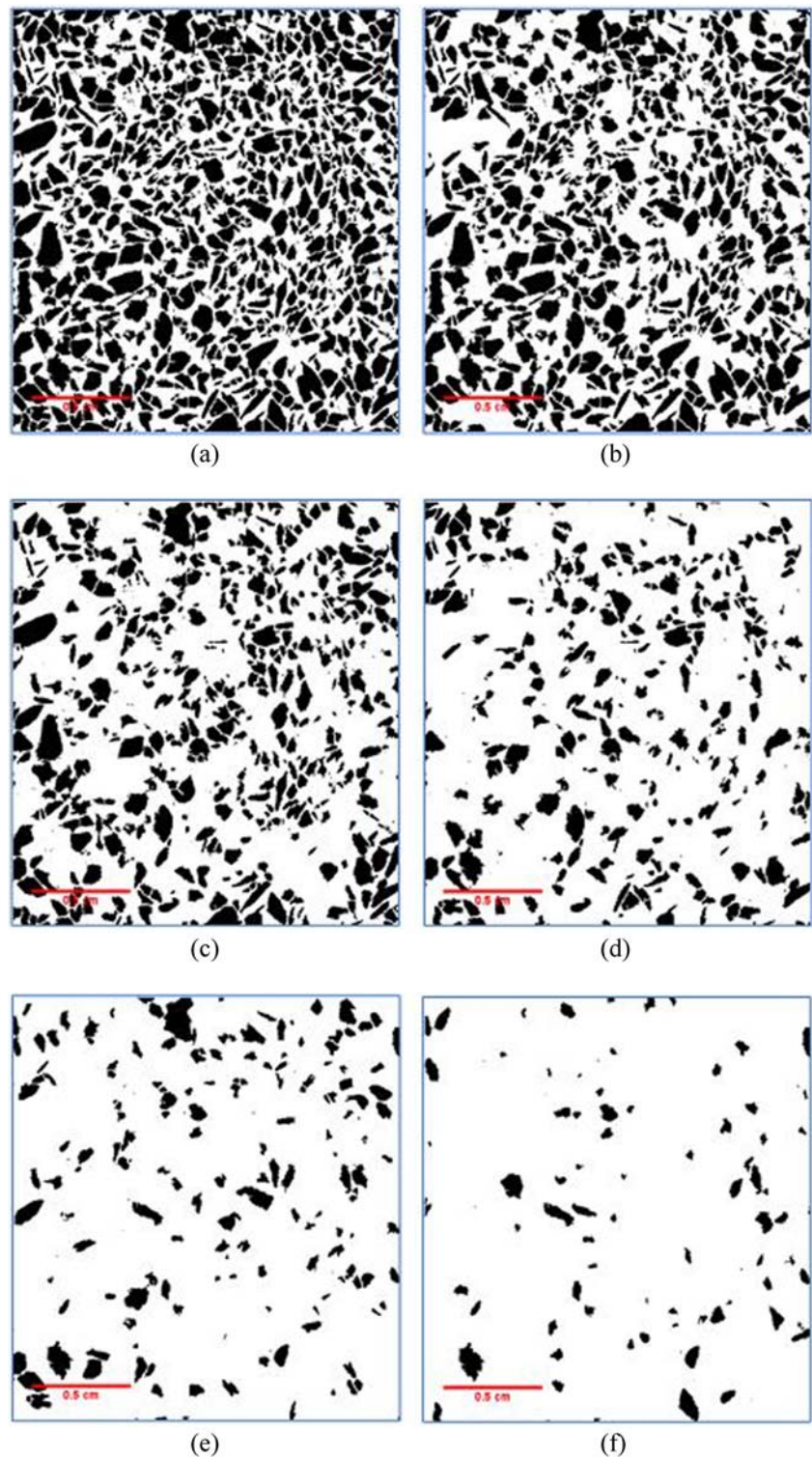
investigate the uncertainty of a V_b estimate when using a scan line. The V_b of physical bimrock models ranged from 13 to 55%. The particle size distribution followed a specific fractal dimension (Medley 1997), which was in agreement with the particle size distribution (PSD) of mélanges from San Francisco. However, the PSD was for 3D bimrock features. Hence, obtaining the D_e from a 3D PSD is necessary.

If a surface cuts though a 3D monodisperse block inclusion, then D_e can be calculated from Eq. (19) as follows:

Fig. 13 Comparison of the *CV*s of block volume fractions: experimental data, analytical solutions, and numerical solution
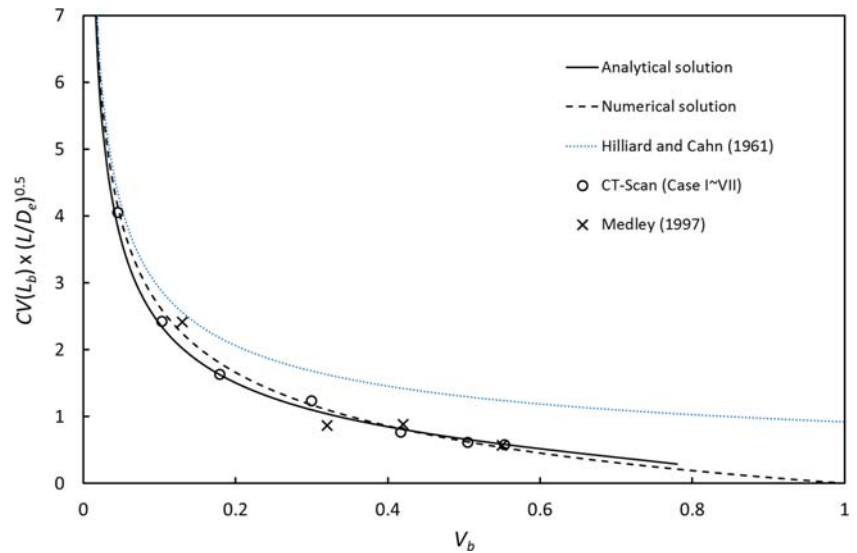
$$D_\text{e} = \int Df(\text{d})d\text{d} = \frac{9\pi}{32}D_{3\text{D}}, \qquad (26)$$

where

$$f(\text{d}) = \frac{\pi\text{d}^2/4}{\pi D_{3\text{D}}^3/6}$$

$$\begin{cases} \text{d} = 2\sqrt{\dfrac{D_{3\text{D}}^2}{4} - x^2}, & \dfrac{-D_{3\text{D}}}{2} \leq x \leq \dfrac{D_{3\text{D}}}{2} \\ \text{d} = 0, & \text{else} \end{cases} \qquad (27)$$

in which $D_{3\text{D}}$ is the block diameter in a 3D feature.

If a surface passes though the 3D polydisperse inclusion, then, by substituting Eq. (26) into Eq. (18), and using a *PSD* for the expression, the following is obtained:

$$D_\text{e} = \frac{9\pi}{32}\int D_{3\text{D}}f(\text{d}_\text{PSD})d\text{d}_\text{PSD} \qquad (28)$$

where $f(\text{d}_\text{PSD})$ represents a *PSD* function.

Medley's (1997) physical model included five different elliptical block sizes, whose minor, middle, and major semi

Table 4 Measured intercept lengths of the illustration of the scan-line method (Kuo 2005)

| Intercept number	Intercept length (cm) Scan-line no.										
	1	2	3	4	5	6	7	8	9	10	11
1	5.7	6.2	1.1	3	4.2	5.3	4.2	4.7	4.2	2.5	4.5
2	3.6	2.1	2.15	1.7	4.1	3.2	1.8	1.05	5.3	3.8	1.25
3	9.3	4.9	5.8	2.8	1.35	1.3	2.1	9.1	1.3	4.8	7.5
4	3.2	1.1	4.1	4.7	2.7	7.5	11.5	4.7	3.7	4.5	3.1
5	3.5	3.4	5.1	3.5	2.4	5.6	4.6	2.7	4.85	3.7	5.6
6	4.2	3.0	2.7	2.9	3.7	3.3	3.15	2.8	6.8	4.4	0.65
7	5.6	9.2		2.8	3.6	3	3.6	3.8	2.1	4.3	2.9
8		4.4			5.7	5.8		3.2	0.8	3.5	3.3
9		5.1			3.1				3.1	2.9	3
10		4.75							3.7	3.2	4.1
11										2.65	5.5
12											2.1
13											1.2
Total	35.1	44.15	20.95	21.4	30.85	35	30.95	32.05	35.85	40.25	44.7
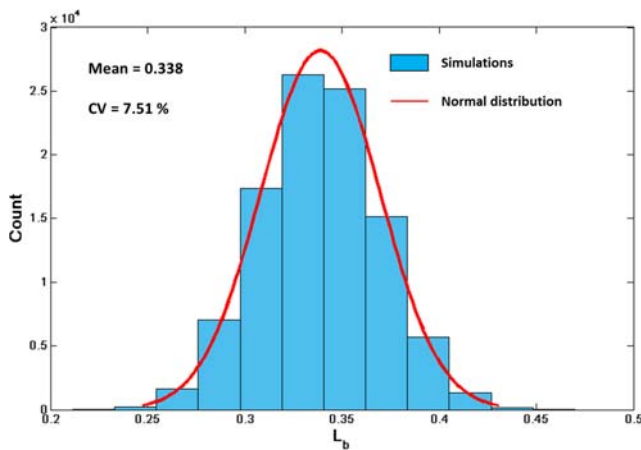
Fig. 14 Histogram of numerical simulation results for L_b for the case of $V_b = 0.338$, $D_e = 6.29$ cm, and $L = 1100$ cm

axes were respectively 3, 3, and 6 mm; 6, 6, and 12 mm; 12, 12, and 24 mm; 24, 24, and 48 mm; and 48, 48, and 96 mm, respectively. If the orientation of an elliptical block follows uniformly random conditions, then the 1D measurement results (mean and uncertainty) will be close to the spherical block dispersion (Tien et al. 2011). The elliptical blocks can be represented as an effective sphere, which has the same volume as the ellipsoids. A *PSD* of the blocks in Medley's physical model is shown in Fig. 9.

After substituting the *PSD* (Fig. 9) into Eq. (28), the equivalent block diameter, D_e, is equal to 32.5 mm. The detailed calculations are shown in Table 2.

Furthermore, this work compares the proposed analytical solution with Eq. (24), the numerical simulation, and Medley's model. The results indicate that the proposed solution is in good agreement with Medley's physical model tests, as shown in Fig. 10 and Table 3.

CT scan images

This study uses a CT scan to obtain internal cross-section images from Iceland sand and crushed rock.

Iceland sand

This sample consists of Iceland sand and an epoxy matrix (Gräser, *personal communication*). The resolution of case

Table 5 The elastic parameters of laterite-gravel formation (Lin 1986)

	Bulk modulus, K (GPa)	Shear modulus, G (GPa)
Laterite	0.0243	0.0112
Gravel I	27.0	12.5

I is 669 pixels × 669 pixels, corresponding to a real size of 6.21 mm × 6.21 mm. The original CT scan images are in grayscale. To separate the block and matrix more clearly, the grayscale images are enhanced to binary images through image processing (shown in Fig. 11). A scan-line analysis code (*SAC*) was developed to detect which blocks would be intersected by scan-lines under binary images. The number of scan lines in the *SAC* depends on the image resolution, i.e., if there are 669 pixels in the horizontal direction, then there will be 669 scan lines in the vertical direction. The *SAC* records the "linear fraction of block" from each scan line and the "intercept length" from each intercepted block.

In case I, the scan-line length, L, is 6.21 mm, and 669 scan lines are generated in the SAC. The SAC also recorded 12,511 intercept lengths, which can be substituted into Eq. (21), and $D_e = 0.366$ mm. A mean of $L_b = 55.4\%$ and a standard deviation of $L_b = 7.83\%$ were obtained.

Comparisons of Hilliard and Cahn's (1961) analytical solution (Eqs. (2) or (3)), the proposed analytical solution, and the numerical solution are shown in Table 3. They indicate that the proposed analytical and numerical solutions agree well with statistical results from case I.

Crushed rock

This sample consists of crushed rock (from Kaoping River, Taiwan) and an epoxy matrix, identified as case II (Fig. 12a). The image size is 483 pixels × 483 pixels, and its physical size is 1.95 cm × 1.95 cm. Both cases I and II are high V_b (more than 50%) images. To obtain images (cases III–VII) with low V_b, a computer program was used to delete blocks in case II randomly, as shown in Fig. 12b–f.

Comparisons of the *CV*s of the block volume fraction for the CT scan images, Hilliard and Cahn's (1961) analytical solution, and the present study are made in Table 3 and Fig. 13. It can be clearly seen that the proposed analytical solution and the numerical solution compare very well with the measured data. However, Hilliard and Cahn's (1961) solution will overestimate in higher V_b conditions.

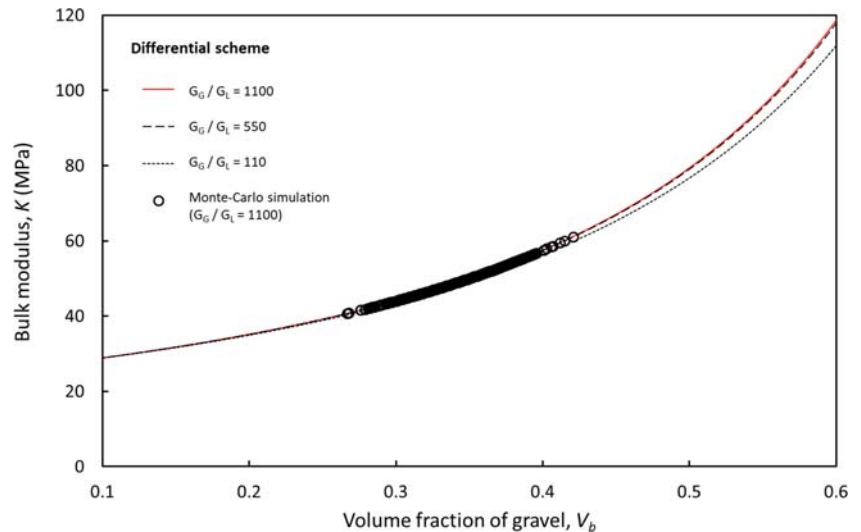## Applications of scan-line measurements

Volume fraction estimation

The location shown in the illustration of the scan-line method is at + 17 km, No. 114 Provincial Highway, Taoyuan County, Taiwan. The geology of this location is

Fig. 15 The bulk modulus of laterite-gravel formation vs volume fraction of block

a laterite-gravel formation (Kuo 2005). The laterite-gravel formation in Taoyuan consists of matric laterite and gravel. The size of the sampling region is 1 m × 1 m, and the total length of the scan line is 11 × 1 m = 11 m, as shown in Fig. 1b (called case VIII). The boundary of the block and matrix is 32 mm (Church et al. 1987).

The intercept lengths of the blocks are shown in Table 4. From this table, L_b can be obtained as follows:

$$L_b = \frac{\sum L_c}{L} = \frac{371.8 \text{ cm}}{1100 \text{ cm}} = 0.338. \tag{29}$$

After substituting the L_c data into Eq. (21), D_e can be determined using:

$$D_e = \frac{4}{\pi} E(L_c) = \frac{4}{\pi} \times \frac{474.3 \text{ cm}}{96} = 6.29 \text{ cm}, \tag{30}$$

Then, by substituting L_b, D_e, and L into Eq. (24), the following is obtained:

$$
\begin{aligned}
CV(L_b)\sqrt{\frac{L}{D_e}} &= \sqrt{\frac{8}{3\pi E(L_b)}} - \sqrt{\frac{\pi}{4E(L_b)}} \\
\Rightarrow CV(L_b)\sqrt{\frac{1100 \text{ cm}}{6.29 \text{ cm}}} &= \sqrt{\frac{8}{3\pi \times 0.338}} - \sqrt{\frac{\pi}{4 \times 0.338}} \\
\Rightarrow CV(L_b) &= 0.0751
\end{aligned} \tag{31}
$$

According to a numerical simulation of this case, the histogram of the linear fractions of the rock is approximately a normal distribution, as shown in Fig. 14. The standard deviation is equal to 0.0254. The 95% confidence interval of L_b is $0.338 \pm 2 \cdot 0.0254$. Based on the data of the scan-line field measurement, the equivalent

Fig. 16 The shear modulus of laterite-gravel formation vs volume fraction of block
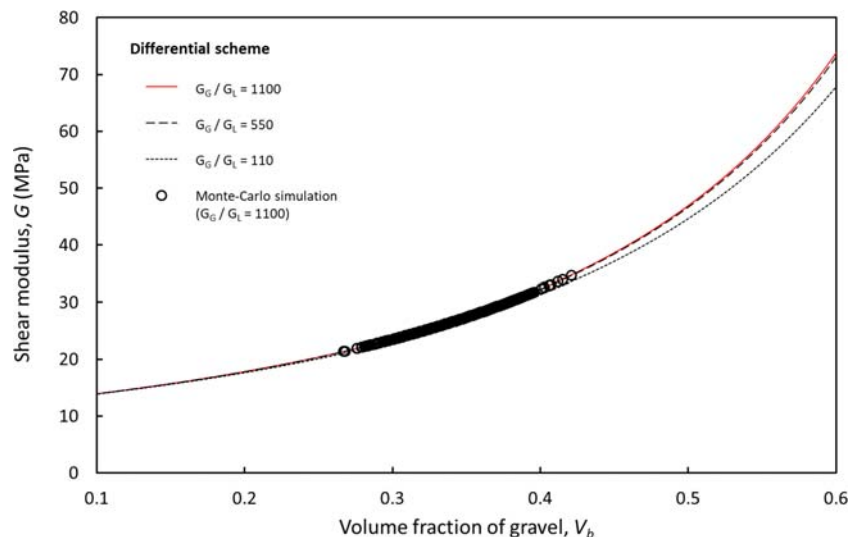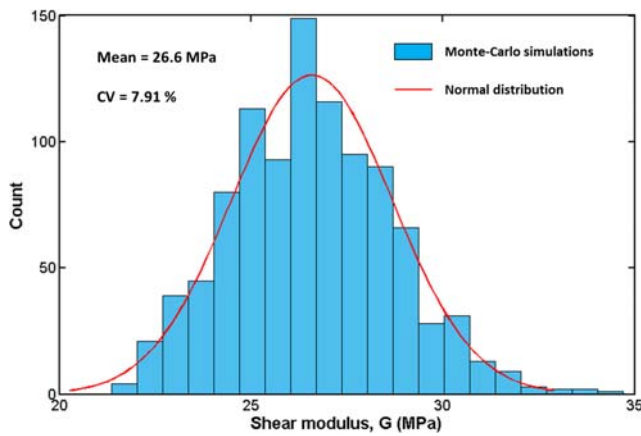
Fig. 17 Histogram of shear modulus of laterite-gravel formation

diameter of the blocks is 6.29 cm. According to the Delesse principle (1847), the expected V_b is 0.338 with a 95% confidence level in the interval of 0.287 to 0.389. In most geotechnical parameter investigations, $CV < 10\%$ corresponds to "low variability" (Phoon et al. 1995). However, if the acceptable CV is more tolerant, e.g., $CV = 20\%$, then the requirement is $L = 1.55$ m.

Estimation of deformability parameters (shear modulus and Young's modulus)

It is generally difficult to determine the deformability of laterite-gravel by conventional laboratory and field tests. The deformability of laterite-gravel may be calculated based on micromechanics, for example, self-consistent scheme (Hershey 1954; Hill 1965) and differential scheme (McLaughlin 1977). The required input parameters for micromechanics include bulk moduli (K) and shear moduli (G) of laterite and gravel (Lin 1986) (as shown in Table 5) and V_f of gravel (denoted herein as V_b). The elastic ratio of gravel and laterite, G of gravel over G of

Fig. 18 Histogram of Young's modulus of laterite-gravel formation

laterite (G_G/G_L) or K of gravel over K of laterite (K_G/K_L), are about 1100. The elastic modulus ratio (Young's modulus over uniaxial compressive strength (E_G/UCS_G) is about 500. Based on the data from the scan-line measurement of case VIII (in section 4.1), the mean and CV of V_b are 0.338 and 0.0751, respectively.

In this paper, we utilize differential scheme (Eq. (32) to Eq. (33)) assuming V_b as a normal random variable and using Monte Carlo approach.

$$\frac{d\overline{K}}{dV_b} = \left(\frac{K_G - \overline{K}}{1 - V_b}\right)\left(\frac{\overline{K} + K^*}{K_G + K^*}\right), \tag{32}$$

$$\frac{d\overline{G}}{dV_b} = \left(\frac{G_G - \overline{G}}{1 - V_b}\right)\left(\frac{\overline{G} + G^*}{G_G + G^*}\right), \tag{33}$$

where

$$K^* = \frac{4}{3}\overline{G}, \ G^* = \frac{\overline{G}\left(9\overline{K} + 8\overline{G}\right)}{6\left(\overline{K} + 2\overline{G}\right)} \text{ for spherical inclusion.}$$

Substitute K_L (which is equal to $\overline{K}$ when $V_b = 0$), G_L (which is equal to $\overline{G}$ when $V_b = 0$), K_G, G_G, and the normal random variable V_b into the differential scheme (McLaughlin 1977). Then, using the 4th order Runge-Kutta method (Butcher 1996) to solve the partial differential equations of the differential scheme, the bulk modulus, $\overline{K}$, and shear modulus, $\overline{G}$, of laterite-gravel formation under a specific V_b value can then be obtained. The simulation results of bulk modulus and shear modulus are shown in Figs. 15 and 16, respectively. The result shows that the influence of stiffness of gravel is insignificant on the overall deformability of laterite-gravel mixture. In addition, Young's modulus (E) and Poisson ratio (υ) can be also obtained by substituting bulk modulus and shear modulus into Eq. (34) and Eq. (35).

$$E = \frac{9\overline{K}\,\overline{G}}{3\overline{K} + \overline{G}}, \tag{34}$$

$$\upsilon = \frac{3\overline{K} - 2\overline{G}}{2\left(3\overline{K} + \overline{G}\right)}. \tag{35}$$

Shear modulus and Young's modulus are important design parameters in geological engineering. The histograms of shear modulus and Young's modulus obtained in this study are shown in Figs. 17 and 18, respectively. These histograms indicate that both design parameters follow approximately normal distribution. The mean and CV of shear modulus and Young's modulus are shown in Table 6, which can provide an estimate of the 95% confidence interval of shear modulus in the range of 22.4 to
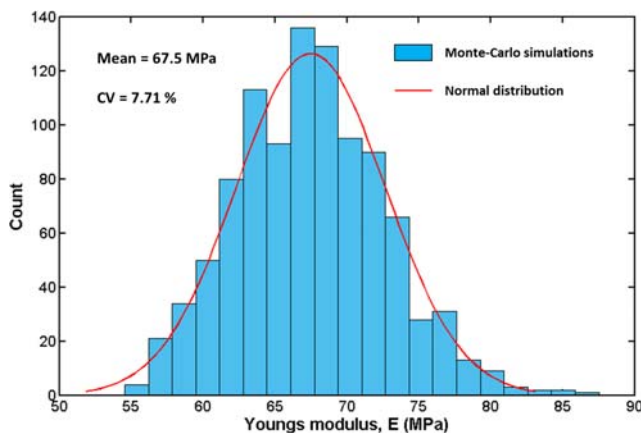
Table 6 The simulation results of elastic moduli of laterite-gravel

L/D_e	Mean of V_b	CV of V_b (%)	Mean of K (MPa)	CV of K (%)	Mean of G (MPa)	CV of G (%)	Mean of E (MPa)	CV of E (%)	Mean of ν	CV of ν (%)
175	0.338	7.51	48.7	6.62	26.6	7.91	67.5	7.71	0.269	0.926
30	0.338	18.1	48.7	15.7	26.5	18.6	67.3	18.2	0.271	2.02

30.8 MPa, and Young's modulus in the range of 57.1 to 77.9 MPa.

It should be noted that the deformability of bimrocks/bimsoils often exhibits spatial and tempo variations (Chen et al. 2019). These variations may be induced by the geometry of bimrocks/bimsoils such as the volume fraction of block. With the proposed approach, the variation of the deformability parameters can be estimated, and the results may be used, for example, for reliability-based design of engineering systems in the bimrocks/bimsoils (Chen et al. 2019).

Summary and conclusions

This paper presented analytical and numerical solutions to quantify the uncertainty of volume fraction measurements in bimrock/bimsoil using a scan-line method. The proposed method had been validated using published physical experimental data and analytical solutions. As the volume fraction estimated with the scan-line measurements is linked to deformability parameters, such as modulus of elasticity and shear modulus, an estimate of these parameters along with their uncertainty characteristics can readily be made. Such information enables the deterministic, as well as the reliability-based, analysis and design of engineering systems in the bimrocks/bimsoils.

I. This paper proposed an analytical solution to quantify the uncertainty of volume fraction estimation in a bimrock/bimsoil using a scan-line method. A geometry model based on representative volume elements was adapted to derive the uncertainty of the volume fraction of a block. The solution is a function of the volume fraction of the block (V_b), the diameter of the block, and the length of the scan line. The applicable range of V_b is between 0 and $\pi/4$.

II. For the numerical approach, a 2D domain was generated, which used a "periodic boundary" to avoid the "wall effect." The results of the numerical simulations agreed well with the analytical solution.

III. Experimental results of the physical model and CT scan images were adapted to validate the analytical and numerical solutions. The proposed analytical and numerical solutions showed a good agreement with the experiments.

IV. The proposed analytical solution for estimation of the volume fraction is further extended into a deterministic micromechanical model to estimate the mean and variation of bimrock's mechanical properties such as the shear modulus and Young's modulus. The variation of these deformability parameters is also characterized.

References

Afifipour M, Moarefvand P (2014a) Mechanical behavior of bimrocks having high rock block proportion. Int J Rock Mech Min Sci 65:40–48

Afifipour M, Moarefvand P (2014b) Failure patterns of geomaterials with block-in-matrix texture: experimental and numerical evaluation. Arab J Geosci 7:2781–2792

ASTM (2012) Standard test method for microscopical determination of parameters of the air-void system in hardened concrete. ASTM, Pennsylvania

Barbero M, Bonini M, Borri-Brunetto M (2008) Three-dimensional finite element simulations of compression tests on bimrock. The 12th International Conference of International Association for Computer Methods and Advances in Geomechanics, Goa, India

Bentz DP, Garboczi EJ (1999) Computer modeling of the interface transition zone – microstructure and properties. RILEM ETC, pp 349-385

Butcher JC (1996) A history of Runge-Kutta methods. Appl Numer Math 20:247–260

Chen F, Wang L, Zhang W (2019) Reliability assessment on stability of tunneling perpendicularly beneath an existing tunnel considering spatial variabilities of rock mass properties. Tunn Undergr Space Technol 88:276–289

Church MA, Mclean DG, Wolcott JF (1987) River bed gravel: sampling and analysis. In: Thorne CR, Bathurst JC, Hey RW (eds) Sediment Transport in Gravel River. Wiley, New York, pp 43–79

Coli N, Berry P, Boldini D (2011) In situ non-conventional shear tests for the mechanical characterization of a bimrock. Int J Rock Mech Min Sci 48:95–102

Coli N, Berry P, Boldini D, Bruno R (2012) The contribution of geostatistics to the characterisation of some bimrock properties. Eng Geol 137-138:53–63

Delesse MA (1847) Procédé mécanique pour déterminer la composition des roches. Comptes Rendues de I'Academie des Sciences 25:544–545

Gokceoglu C (2002) A fuzzy triangular chart to predict the uniaxial compressive strength of the Ankara Agglomerates from their petrographic composition. Eng Geol 66:39–51

Hershey AV (1954) The elasticity of an isotropic aggregate of anisotropic cubic crystals. J Appl Mech 21:236

Hill R (1965) A self-consistent mechanics of composite materials. J Mech Phys Solids 13:213–222

Hilliard JE, Cahn JW (1961) An evaluation of procedures in quantitative metallography for volume-fraction analysis. Trans Metall Soc AIME 221:344–352

Holmes A (1921) Petrographic methods and calculations. Thos. Murray and Co., London

Kahraman S, Alber M (2006) Estimating the unconfined compressive strength and elastic modulus of a fault breccia mixture of weak rocks and strong matrix. Int J Rock Mech Min Sci 43:1277–1287

Kahraman S, Alber M (2008) Triaxial strength of a fault breccia of weak rocks in a strong matrix. Bull Eng Geol Environ 67:435–441

Kahraman S, Alber M (2009) Predicting the uniaxial compressive strength and elastic modulus of a fault breccia from texture coefficient. Rock Mech Rock Eng 42:117–127

Kahraman S, Alber M, Fener M, Gunaydin O (2015) An assessment on the indirect determination of the volumetric block proportion of Misis fault breccia (Adana, Turkey). Bull Eng Geol Environ 74:899–907

Kalender A, Sonmez H, Medley E, Tunusluoglu C, Kasapoglu KE (2014) An approach to predicting the overall strengths of unwelded bimrocks and bimsoils. Eng Geol 183:65–79

Krumbein WC, Pettijohn FJ (1938) Manual of sedimentary petrography. Appleton-century Company, New York

Kuo MC (2005) The measurement of block volumetric fraction and the mechanical behaviors of composite rock mass. Dissertation, Department of Civil Engineering, National Central University, Taoyuan, Taiwan

Lin PS (1986) A study on engineering properties of compacted lateritic gravels. J Chin Inst Eng 9:533–545

Lindquist ES (1994) The strength and deformation properties of Mélange. Dissertation, Department of Civil Engineering, University of California, Berkeley, USA

Lindquist ES, Goodman RE (1994) The strength and deformation properties of a physical model melange. In: Nelson PP, Laubach SE (eds) Proceedings of the 1st North American Rock Mechanics Symposium. Balkema, Austin

Liu S, Huang X, Zhou A, Hu J, Wang W (2018) Soil-rock slope stability analysis by considering the nonuniformity of rocks. Mathematical Problems in Engineering 2018:ID 3121604

McLaughlin R (1977) A study of the differential scheme for composite materials. Int J Eng Sci 15:237–244

Medley EW (1994) The engineering characterization of Mélange and similar block-in-matrix-rocks (bimrocks). Dissertation, Department of Civil Engineering, University of California, Berkeley, USA

Medley EW (1997) Uncertainty in estimates of block volumetric proportions in mélange. Proceedings International Symposium on Engineering Geology and Environment. AA Balkema

Medley EW (2001) Orderly characterization of chaotic Franciscan Mélange. Felsbau-Rock Soil Eng 22:27–34

Medley EW, Goodman RE (1994) Estimating the block volumetric proportions of Mélanges and similar block-in-matrix rocks (bimrocks). Proceedings of the 1st North American Rock Mechanics Symposium, Austin, Texas. AA Balkema

Medley EW, Sanz Rehermann PF (2004) Characterization of bimrocks (rock/soil mixtures) with application to slope stability problems. Proceedings: Eurorock 2004 & 53rd Geomechanics Colloquium, Salzburg, Austria

Meng Q, Wang H, Xu W, Zhang Q (2018) A coupling method incorporating digital image processing and discrete element method for modeling of geomaterials. Eng Comput 35(1):411–431

Phoon KK, Kulhawy FH, Grigoriu MD (1995) Reliability-based design of foundations for transmission line structures. Electric Power Research Institute. Report TR-105000

Russ JC, Dehoff RT (1999) Practical stereology. Plenum Press, New York

Sonmez H, Gokceoglu C, Tuncay E, Medley EW, Nefeslioglu HA (2004) Relationships between volumetric block proportions and overall UCS of a volcanic bimrock. Felsbau-Rock Soil Eng 5:27–34

Sonmez H, Gokceoglu C, Medley EW, Tuncay E, Nefeslioglu HA (2006a) Estimating the uniaxial compressive strength of a volcanic bimrock. Int J Rock Mech Min Sci 43:554–561

Sonmez H, Gokceoglu C, Nefeslioglu HA, Kayabasi A (2006b) Estimation of rock modulus: for intact rocks with an artificial neural network and for rock masses with a new empirical equation. Int J Rock Mech Min Sci 43:224–235

Sonmez H, Ercanoglu M, Kalender A, Dagdelenler G, Tunusluoglu C (2016) Predicting uniaxial compressive strength and deformation modulus of volcanic bimrock considering engineering dimension. Int J Rock Mech Min Sci 86:91–103

Stein A, Yifru MZ (2010) Stereological estimation of uncertain and changing objects from remote sensing image mining. Trans GIS 14:481–496

Tien YM, Lin JS, Kou MC, Lu YC, Chung YJ, Wu TH, Lee DH (2010) Uncertainty in estimation of volumetric block proportion of bimrocks by using scanline Method. 44th U.S. Rock Mechanics/Geomechanics Symposium and 5th U.S.-Canada Rock Mechanics Symposium, Salt Lake City. Paper no. 10-158

Tien YM, Lu YC, Wu TH, Lin JS, Lee DH (2011) Quantify uncertainty in scanline estimates of volumetric fraction of anisotropic bimrocks. 45th U.S. Rock Mechanics/Geomechanics Symposium, San Francisco. Paper no. 11-345

Tien YM, Lu YC, Chang HH, Chung YC, Lin JS, Lee DH (2012) Uncertainty of volumetric fraction estimates using 2-D measurements. 46th U.S. Rock Mechanics/Geomechanics Symposium, Chicago. Paper no. 12-494

Tien YM, Lu YC, Hsu KS (2015a) Numerical simulation of the shear behaviors of rock joints under the direct shear test. 49th U.S. Rock Mechanics/Geomechanics Symposium, San Francisco. Paper no. 15-613

Tien YM, Lu YC, Cheng HH (2015b) Variability of mechanical properties of bimrock. 49th U.S. Rock Mechanics/Geomechanics Symposium, San Francisco. Paper no. 15-614

Tsesarsky M, Hazan M, Gal E (2014) Estimating the elastic moduli and isotropy of block inmatrix (bim) rocks by computational homogenization. Eng Geol 200:58–65

Wackerly DD, Mendenhall W III, Scheaffer RL (2008) Mathematical statistics with applications, 7th edn. Thomson Learning Inc.

Xia J, Gao W, Hu R, Sui H (2017) Influence of strength difference between block and matrix on the mechanical property of block-in-matrix soils: an experimental study. Electron J Geotech Eng 22: 2411–2426

Xu WJ, Yue ZQ, Hu RL (2008) Study on the mesostructure and mesomechanical characteristics of the soil–rock mixture using digital image processing based finite element method. Int J Rock Mech Min Sci 45:749–762

Xu WJ, Xu Q, Hu RL (2011) Study on the shear strength of soil-rock mixture by large scale direct shear test. Int J Rock Mech Min Sci 48: 1235–1247

Yang L, Xu W, Meng Q, Xie WC, Wang H, Sun M (2019) Numerical determination of RVE for heterogeneous geomaterials based on digital image processing technology. Processes 7(6):346

Ymeti I, van der Werff H, Shrestha DP, Jetten VG, Lievens C, van der Meer F (2017) Using color, texture and object-based image analysis of multi-temporal camera data to monitor soil aggregate breakdown. Sensors 17:1241

Zhang WG, Zhang RH, Han L, Goh ATC (2019) Engineering properties of Bukit Timah Granitic residual soils in Singapore DTL2 braced excavations. Undergr Space 4(2):98–108